Journal of Advanced Ceramics
2022, **11**(7): 1153–1162
https://doi.org/10.1007/s40145-022-0602-6
ISSN 2226-4108
CN 10-1154/TQ

Research Article

Fabrication, microstructure, and properties of 8 mol% yttria-stabilized zirconia (8YSZ) transparent ceramics

Penghui CHEN[a,b], Xiaoying LI[a,b], Feng TIAN[a,b], Ziyu LIU[a,b], Dianjun HU[a,b], Tengfei XIE[a], Qiang LIU[c], Jiang LI[a,b,*]

[a]*Key Laboratory of Transparent Opto-functional Inorganic Materials*, *Shanghai Institute of Ceramics*, *Chinese Academy of Sciences*, *Shanghai 201899*, *China*
[b]*Center of Materials Science and Optoelectronics Engineering*, *University of Chinese Academy of Sciences*, *Beijing 100049*, *China*
[c]*School of Materials Science and Engineering*, *Jiangsu University*, *Zhenjiang 212013*, *China*

Received: February 11, 2022; Revised: April 2, 2022; Accepted: April 20, 2022

Abstract: Fine grained 8 mol% yttria-stabilized zirconia (8YSZ) transparent ceramics with high optical and mechanical properties were fabricated by air pre-sintering and hot isostatic pressing (HIP) using commercial 8YSZ powders as the raw material. The pre-sintered ceramics with fine grains and appropriate relative density play a key role to achieve high transparency and suppressed grain size after HIP post-treatment at relatively low temperatures. With the increase of HIP temperature from 1350 to 1550 ℃, the in-line transmittance of 8YSZ ceramics at 600 nm increases from 56.9% to 71.5% (2.5 mm in thickness), and the average grain size increases from 2.4 to 16.3 μm. The corresponding bending strength of 8YSZ transparent ceramics decreases from 328±20 to 289±19 MPa, the hardness (H) decreases from 12.9±0.1 to 12.5±0.2 GPa, and the fracture toughness (K_{IC}) decreases from 1.30±0.02 to 1.26±0.03 MPa·m$^{1/2}$. Systematical investigations were carried out to study the combination of high optical transparency and excellent mechanical properties in 8YSZ ceramics.

Keywords: yttria-stabilized zirconia (8YSZ) transparent ceramics; hot isostatic pressing (HIP); microstructure; optical transparency; mechanical properties

1 Introduction

The addition of Y_2O_3 can stabilize the tetragonal and cubic crystal structure of ZrO_2 due to the presence of oxygen vacancies [1,2]. Yttria-stabilized ZrO_2 ceramics show many mechanical and functional advantages, such as high hardness (H), high chemical stability, low thermal conductivity, high oxygen diffusivity, and well-proven biocompatibility [3–5]. Cubic yttria-stabilized ZrO_2 (8 mol% yttria-stabilized zirconia (8YSZ)) transparent ceramics have a high refractive index (n) of ~2.2 [6,7], which is higher than those of most optical glasses and most oxide crystals. Based on these advantages, 8YSZ transparent ceramics are expected to serve as the multifunctional material [8–11], in particular, as optical lenses [12], windows [2], and biomedical prostheses [5,13].

The microstructure with full density or extremely low porosity is basically required to obtain highly

* Corresponding author.
E-mail: lijiang@mail.sic.ac.cn

transparent polycrystalline ceramics, because the micro-pores can work as optical scattering centers to decrease the in-line transmission [10,14–16]. Highly transparent 8YSZ ceramics can be realized only when the porosity is less than 100 ppm, even though the radius of residual pores is smaller than 50 nm [17]. During the pressureless sintering, the driving force (p) for the closure of isolated pores can be calculated from Eq. (1) [18,19]:

$$p = \frac{2\gamma_{sv}}{r} \quad (1)$$

where γ_{sv} is the pore surface energy and r is the curvature radius of the pores. If γ_{sv} is assumed as ~1 J/m^2 and the average pore radius is ~0.2 μm for the pre-sintered 8YSZ ceramics in this case, then p is calculated to be 10 MPa. The typical pressure during hot isostatic pressing (HIP) is 150–200 MPa, which provides 15–20 times driving force for densification greater than that of the normal pressureless sintering. As a consequence, pressureless pre-sintering combined with HIP post-treatment method is frequently employed to fabricate transparent ceramics, because more driving force can be provided during HIP post-treatment to eliminate micro-pores and promote the densification [16,18,20–22]. In 1986, Tsukuma [23] firstly fabricated 8YSZ transparent ceramics by oxygen pre-sintering and HIP post-treatment at 1500 ℃ using commercial 8YSZ powders and 10 mol% TiO_2 as sintering aid. The ceramic sample showed an in-line transmittance of ~60% at 600 nm (0.73 mm in thickness) and the large grain size (> 100 μm). In 2008, Tsukuma *et al*. [17] then obtained 8YSZ transparent ceramics by air pre-sintering and HIP post-treatment at 1650 ℃ using commercial 8YSZ powders. It was indicated that the pre-sintering temperatures had a great influence on the optical transmittance of the HIP post-treated ceramics. In-line transmittance of the 8YSZ ceramic sample was comparable to the single crystals at the wavelength above 600 nm (1 mm in thickness). Nonetheless, the grain size was larger than 50 μm. In 2009, Peuchert *et al*. [12] prepared 10YSZ transparent ceramics by vacuum pre-sintering and HIP post-treatment at 1750 ℃ using commercial 10YSZ powders and 5 wt% TiO_2 as sintering aid. The ceramic sample showed an in-line transmittance of 68% at 600 nm (5.6 mm in thickness) without reporting grain size. In our previous studies [24–26], $Y_{0.16}Zr_{0.84}O_{1.92}$ transparent ceramics were fabricated by air pre-sintering and HIP post-treatment at 1750–1800 ℃ from the nano-powders synthesized by the co-precipitation method. High in-line transmittance (about 70.0% at 600 nm, 1.0 mm in thickness) and large grain size (> 50 μm) were obtained. Owing to the introduction of sintering aid (TiO_2) or high sintering temperatures during HIP post-treatment, the 8YSZ transparent ceramics were characterized by large grain size, and no mechanical properties were reported. It has been shown that the reduced grain size will increase the mechanical properties of ceramics. Spark plasma sintering (SPS) technique is an effective method to obtain nano-grained transparent ceramics due to the relatively low sintering temperatures and short sintering time [1,5,10,27–32]. In 2010–2021, 8YSZ transparent ceramics were fabricated by SPS at the temperature range of 1100–1400 ℃ using commercial 8YSZ powders, as reported in Refs. [1,5,6,10,11]. The average grain size of 8YSZ transparent ceramics was approximately 100 nm; however, the in-line transmittance rapidly decreased in the visible region and was only about 40% at 600 nm (1.0 mm in thickness). Whereas, only simple H or fracture toughness (K_{IC}) of the 8YSZ ceramics was reported. Although the SPS technique can be used to suppress the grain growth, the pores of ceramics cannot be eliminated effectively.

It is reported that the pre-sintered 8YSZ ceramics with fine grains and appropriate relative density can provide higher optical transmittance for the HIP post-treated ceramics [17]. During the stage of solid-state pressure densification, the densification rate ($\frac{\mathrm{d}(\Delta\rho/\rho)}{\mathrm{d}t}$) can be estimated by either Nabarro–Herring or Coble creep from Eq.(2) [18,19]:

$$\frac{\mathrm{d}(\Delta\rho/\rho)}{\mathrm{d}t} = 31.5\frac{\Omega}{kTG^2}(1-\rho)\left(D_v + \frac{\pi\delta D_b}{G}\right)\sigma_a \quad (2)$$

where $\Delta\rho$ is the relative density difference, t is the time, Ω is the molar volume, k is the Boltzmann constant, T is the absolute temperature, G is the average grain size, ρ is the relative density, D_v is the volume diffusion coefficient, δ is the boundary thickness, D_b is the boundary diffusion coefficient, and σ_a is the applied stress. According to Eq. (2), the densification rate of ceramics during HIP post-treatment can be enhanced effectually by minimizing the grain size of pre-sintered samples. Due to the large plastic deformation of fine grains and the rapid migration of small intergranular pores, the HIP temperature can be further decreased [16,33]. Air pre-sintering followed by HIP post-

treatment is an excellent method to achieve 8YSZ transparent ceramics with suppressed grain under relatively low sintering temperatures. In the patent published in 2018, Masahiro *et al*. [34] fabricated 8YSZ transparent ceramics by air pre-sintering and HIP post-treatment at relatively low temperature using commercial 8YSZ powders. For the 8YSZ ceramics HIP post-treated at 1300–1500 ℃, the in-line transmittance at 600 nm increased from 57% to 70% (1.0 mm in thickness), G increased from 0.7 to 5.0 μm, and the bending strength decreased from 432 to 376 MPa. However, to the best of our knowledge, no systematical investigations were carried out to study the combination of high optical and mechanical properties in 8YSZ ceramics so far. Importantly, the reported 8–10YSZ transparent ceramics are all small in size, which cannot meet the requirements for the potential applications.

In this work, we successfully prepared the 8YSZ transparent ceramics possessing high optical transparency and excellent mechanical properties using commercial 8YSZ powders without any sintering additive. The influences of pre-sintering and HIP post-treatment temperature on the microstructure, optical transparency, and mechanical properties of 8YSZ ceramics were systematically studied.

2 Experimental

Commercial 8YSZ granulated powders (grade TZ-8Y, Tosoh Corporation, Japan) were used as the starting materials. The specific surface area of granulated powders is 16±3 m^2/g, and the purity of 8YSZ powders is ZrO_2+HfO_2+Y_2O_3 > 99.7 wt%. The powders were uniaxially dry-pressed into ϕ18 mm and 50 mm × 50 mm disks. After that, the pellets were cold isostatically pressed at 250 MPa. The green bodies were firstly air pre-sintered at 1250–1325 ℃ for 4 h in a muffle furnace. The heating rate was 400 ℃/h from room temperature to 1100 ℃ and maintained at a slow value to the peak temperature. Then, the pre-sintered 8YSZ ceramics were HIP post-treated at 1350–1550 ℃ for 3 h under an Ar atmosphere of 176 MPa.

The crystalline phases of 8YSZ powders were determined by an X-ray diffractometer (D8 Advance, Bruker, Germany) using nickel filtered Cu Kα radiation in the 2θ range of 20°–80°. The morphologies of 8YSZ powders were investigated by a field emission scanning electron microscope (FESEM; SU9000, Hitachi, Japan). The relative densities of the sintered ceramics were measured by the Archimedes method in deionized water, and the theoretical density of 8YSZ ceramics was considered as 5.98 g/cm^3. The microstructures of the thermally-etched surfaces of 8YSZ ceramics were observed by an FESEM (SU8220, Hitachi, Japan). G of sintered ceramics were calculated by the line-intercept method using Eq. (3):

$$G = 1.56L \tag{3}$$

where L is the average linear intercept distance. The in-line transmission spectra of 8YSZ transparent ceramics were measured by an ultraviolet–visible–near infrared (UV–Vis–NIR) spectrophotometer (Cray-5000, Varian, USA) in the wavelength range of 200–850 nm.

The bending strength of 8YSZ transparent ceramics was determined by the three-point loading method using a universal testing machine (Instron-5566, Instron, USA). The test bars with the dimensions of 3 mm × 4 mm × 36 mm were prepared from the 8YSZ transparent ceramics. The Vickers hardness was assessed on polished 8YSZ ceramic surfaces by the indentation method using a hardness testing machine (Tukon-2100B, Instron, USA). H was determined as

$$H = n(P/d^2) \tag{4}$$

where P is the load on the indenter (9.806 N); d is the indentation diagonal; and n is the coefficient dependent on the indenter shape, which is 1.891 in this case. K_{IC} was expressed as

$$K_{IC} = 0.016\left(\frac{E}{H}\right)^{1/2}\left(\frac{P}{C^{3/2}}\right) \tag{5}$$

where E is the Young's modulus, which is considered to be 220 GPa [2]; and C is the linear dimensions of the radial cracks.

3 Results and discussion

Figure 1 shows the X-ray diffraction (XRD) pattern of the commercial 8YSZ powders. The characteristic diffraction peaks of 8YSZ powders are well indexed as the reference pattern of 8YSZ phase (PDF#30-1468). The small peak at 2θ = 28.2° is related to the monoclinic ZrO_2 phase. The average crystalline size (D_{XRD}) of the 8YSZ powders can be calculated by the Scherrer's formula:

$$D_{XRD} = \frac{0.89\lambda}{\beta \cdot \cos\theta} \tag{6}$$

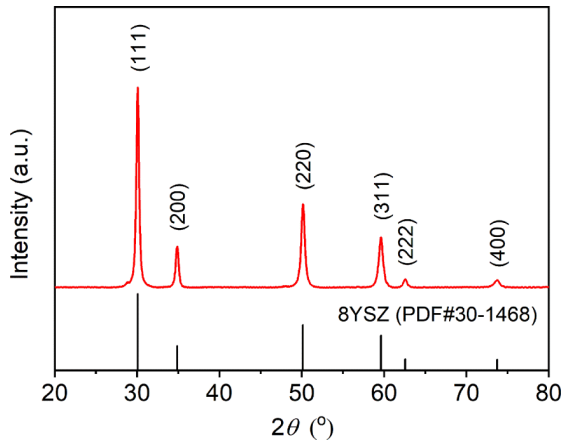

Fig. 1 XRD pattern of the commercial 8YSZ powders.

where λ is the wavelength of X-ray (λ = 1.542 Å), β is the full width at half-maximum (FWHM) of diffraction peak, and θ is the Bragg angle. The D_{XRD} of the 8YSZ powders is calculated to be 21.6 nm.

Figure 2(a) presents the micrograph of the 8YSZ granulated powders. It can be seen that the granulated powders have homogeneous and mono-dispersed spherical particles, whose particle size ranges from few to 60 μm. Figure 2(b) presents the micrograph of the enlarged surface of spherical particles, and Fig. 2(c) shows the particle size distribution of 8YSZ powders. The particle size distribution of the 8YSZ powders ranges from 20 to 300 nm with the maximum proportion in the range of 50–75 nm.

Figure 3 depicts the thermally-etched surfaces of the 8YSZ ceramics pre-sintered at 1250, 1275, 1280, 1290, 1300, and 1325 ℃ for 4 h in air. To expose the grain boundaries, the pre-sintered ceramics were thermally etched at 1100 ℃ for 3 h in a muffle furnace. The relative densities and average grain sizes of 8YSZ

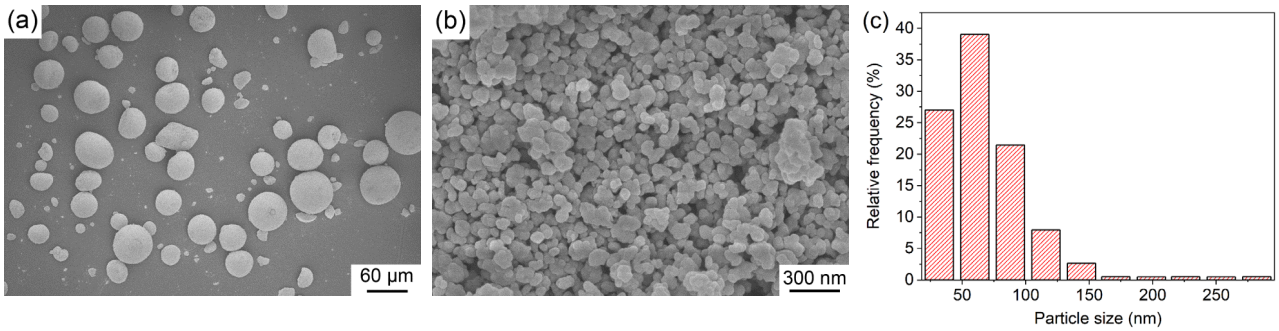

Fig. 2 FESEM micrographs of (a) the granulated 8YSZ powders and (b) the enlarged surface of spherical particles; and (c) the particle size distribution of 8YSZ powders.

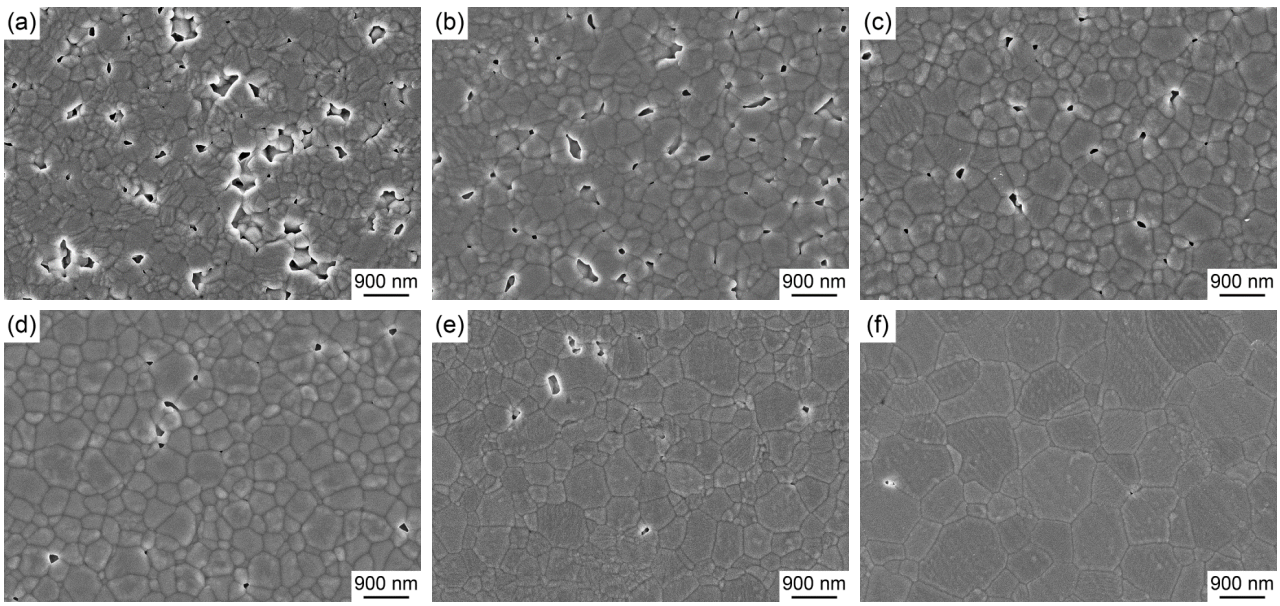

Fig. 3 FESEM micrographs of the thermally-etched surfaces of 8YSZ ceramics pre-sintered at (a) 1250 ℃, (b) 1275 ℃, (c) 1280 ℃, (d) 1290 ℃, (e) 1300 ℃, and (f) 1325 ℃ for 4 h in air.

ceramics as functions of the pre-sintering temperatures are shown in Fig. 4, and the densification behavior can be divided into three stages in the temperature range of 1250–1275, 1275–1290, and 1290–1325 ℃. In the first stage (1250–1275 ℃), which is masked as the blue area in Fig. 4, the relative densities of pre-sintered 8YSZ ceramics are less than 90%, and the average grain size increases slightly from 0.41 to 0.52 μm. As shown in Figs. 3(a) and 3(b), many interconnected sub-micropores as well as some closed pores can be observed. The connections between interconnected sub-micropores tend to be broken away with the further increase of temperature, leading to pore isolation [33]. In the second stage (1275–1290 ℃) which is masked in orange, the relative density increases obviously from 89.0% to 93.9%, and the average grain size increases from 0.52 to 0.61 μm when the pre-sintering temperature increases from 1275 to 1280 ℃. For the 8YSZ ceramic sample pre-sintered at 1280 ℃, the number of residual pores decreases, and only some isolated intergranular sub-micropores are observed in Fig. 3(c). The isolated pores have less pinning effect than the interconnected pores which can efficiently suppress the grain growth [33]. Compared with the ceramic sample pre-sintered at 1275 ℃, only part grains significantly grow in the 1280 ℃ pre-sintered ceramic sample, while many grains remain small size. The 8YSZ ceramic sample pre-sintered at 1280 ℃ provides the optimum microstructure for HIP post-treatment. When the pre-sintering temperature increases to 1290 ℃, slight growth occurs for the small grains, and the residual pores are gradually removed (Fig. 3(d)). In the third stage (1290–1325 ℃) which is masked in green, the relative densities exceed 97%, and the average grain size shows a rapid increase from 0.63 to 1.28 μm. As shown in Figs. 3(e) and 3(f), the residual micro-pores are further eliminated.

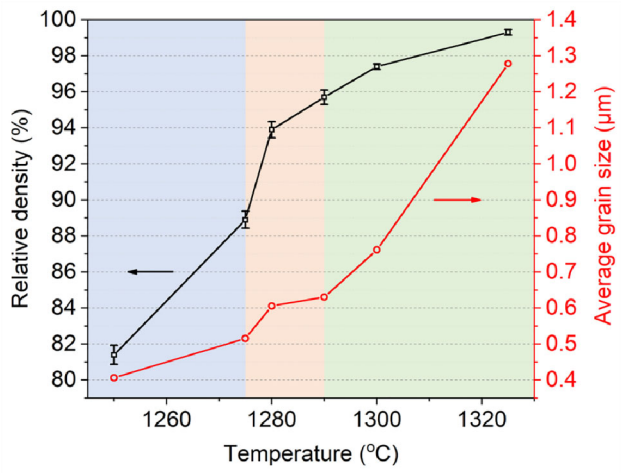

Fig. 4 Relative densities and average grain sizes as functions of air pre-sintering temperature for 8YSZ ceramics (holding time = 4 h).

Figure 5 exhibits the photographs of the double-side polished 8YSZ ceramics (2.5 mm in thickness) pre-sintered at 1250–1325 ℃ for 4 h and further HIP post-treated at 1350, 1450, and 1550 ℃ for 3 h. The transparency of these ceramic samples is strongly influenced by the temperatures of pre-sintering and HIP post-treatment. All the ceramic samples pre-sintered at 1250 and 1275 ℃ are opaque. All the ceramic samples pre-sintered at 1280–1300 ℃ exhibit high transparency and the letters behind these samples can be clearly observed. Inversely, translucency arises in the 8YSZ ceramic samples pre-sintered at 1325 ℃ and HIP post-treated at 1350 and 1450 ℃. Furthermore, the letters under the ceramics become clear gradually as the HIP temperature increases from 1350 to 1550 ℃. Notably, the dark appearance of 8YSZ transparent ceramics is related to the absorption of incident light by oxygen vacancies. During the HIP treatment, the inert atmosphere and graphite heater at high temperatures create a reducing environment with a certain degree, which leads to the formation of oxygen vacancies. Annealing in oxidizing atmosphere can reduce the oxygen vacancies of 8YSZ transparent ceramics and increase the brightness. However, the compressed pores produced by HIP treatment may expand after annealing and reduce the optical transparency at short-wave [35]. Further researches are needed in the future to study the influence of annealing on the HIP post-treated 8YSZ ceramics.

Figure 6 illustrates the in-line transmission curves of the 8YSZ ceramics (2.5 mm in thickness) pre-sintered

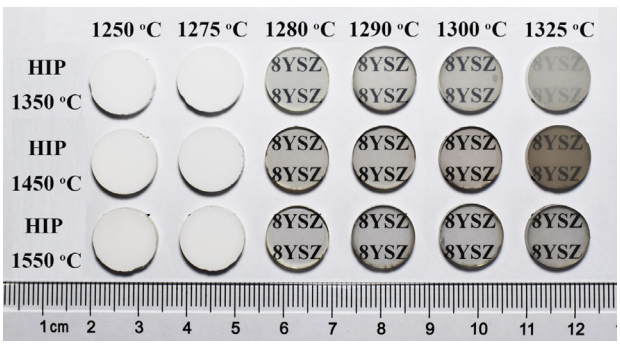

Fig. 5 Photographs of the 8YSZ ceramics (2.5 mm in thickness) pre-sintered at 1250–1325 ℃ for 4 h in air and then HIP post-treated at 1350, 1450, and 1550 ℃ for 3 h under 176 MPa Ar.

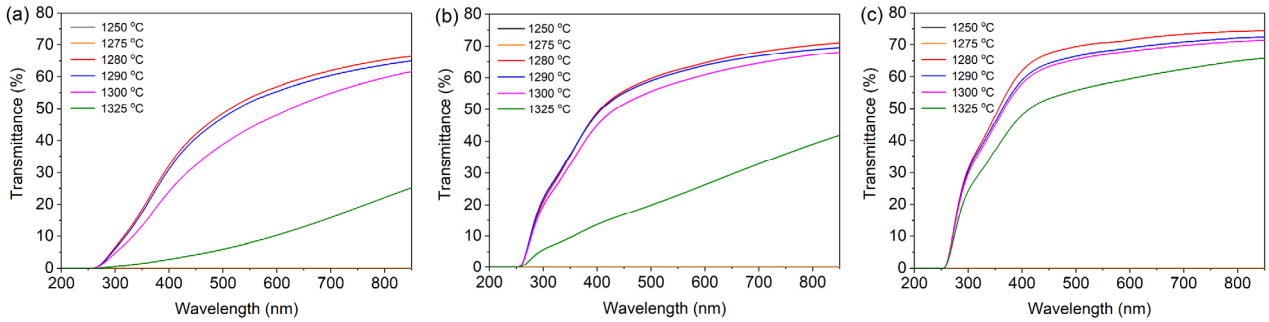

Fig. 6 In-line transmission curves of the 8YSZ ceramics (2.5 mm in thickness) pre-sintered at 1250, 1275, 1280, 1290, 1300, and 1325 ℃ for 4 h and then HIP post-treated at different temperatures for 3 h under 176 MPa in Ar at (a) 1350 ℃, (b) 1450 ℃, and (c) 1550 ℃.

at different temperatures for 4 h and HIP post-treated at 1350, 1450, and 1550 ℃ for 3 h. The in-line transmittances of HIP post-treated ceramics pre-sintered at 1250 and 1275 ℃ are very low due to the opaqueness of the samples. The in-line transmittance reaches the maximum when the pre-sintering temperature is 1280 ℃ and gradually decreases with the increase of pre-sintering temperature. As the HIP temperature increases from 1350 to 1550 ℃, the in-line transmittances of 8YSZ transparent ceramics have a remarkable improvement. The absorption band around 350 nm is caused by the oxygen vacancy defects produced during HIP post-treatment. With the increase of HIP post-treatment temperature from 1350 to 1550 ℃, the concentration of oxygen vacancy increases and the absorption band is more obvious. For the 8YSZ ceramics pre-sintered at 1280 ℃ and then HIP post-treated at 1350, 1450, and 1550 ℃, the in-line transmittances at 600 nm are 56.9%, 64.7%, and 71.5%, respectively. The theoretical transmittance (T_{theory}) of transparent ceramics can be calculated from Eq. (7) [36]:

$$T_{\text{theory}} = 2n/(n^2+1) \tag{7}$$

where n of transparent 10YSZ ceramics is 2.161 at 633 nm [12], and the corresponding T_{theory} is calculated to be 76.2%, which is close to that of 8YSZ transparent ceramics. Additionally, the in-line transmittances of the 8YSZ transparent ceramics gradually decrease with decreasing the wavelength, which can be attributed to the residual micro-pores in the ceramic samples and the oxygen vacancy defects [37].

Figure 7 gives the thermally-etched surfaces of the

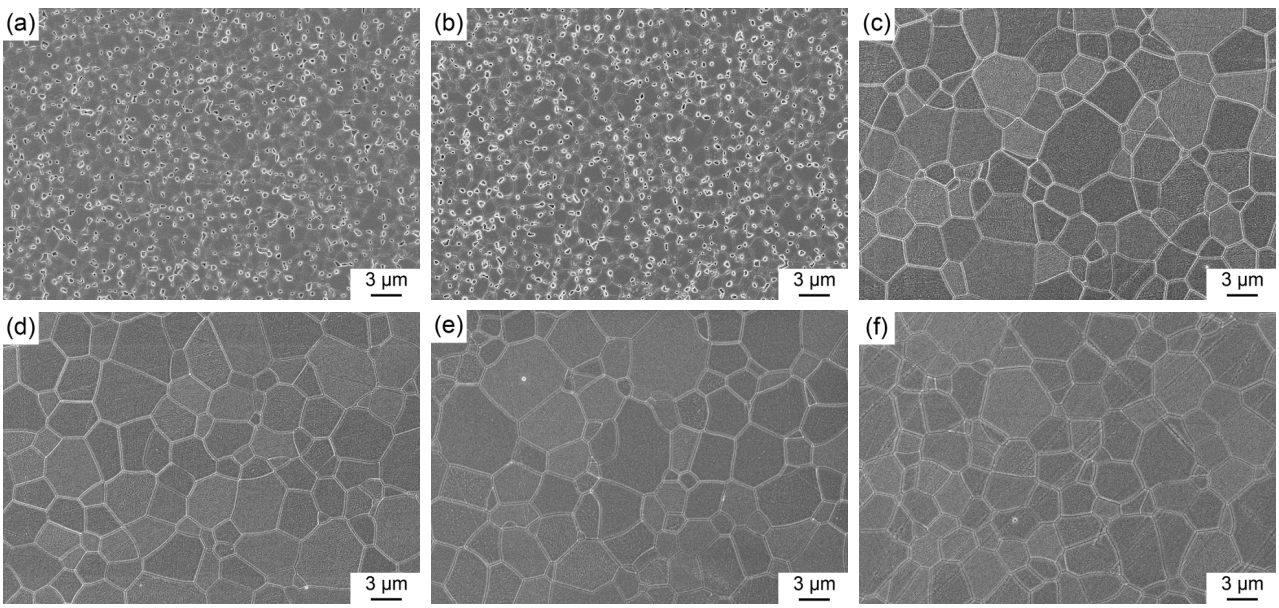

Fig. 7 FESEM micrographs of the thermally-etched surfaces of 8YSZ ceramics pre-sintered at different temperatures for 4 h in air and HIP post-treated at 1450 ℃ for 3 h under 176 MPa Ar at: (a) 1250 ℃, (b) 1275 ℃, (c) 1280 ℃, (d) 1290 ℃, (e) 1300 ℃, and (f) 1325 ℃.

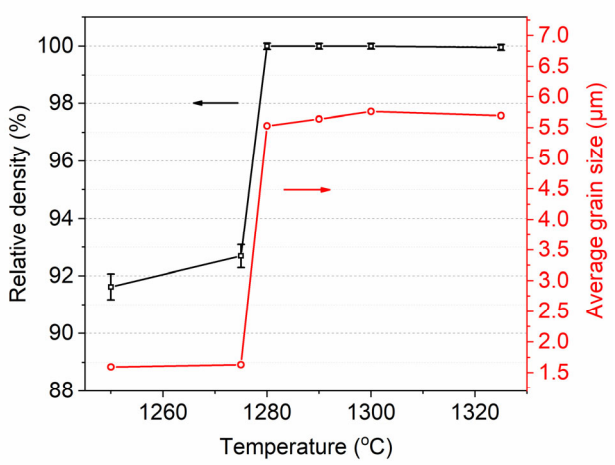

Fig. 8 Relative densities and average grain sizes of the 8YSZ ceramics after HIP post-treatment at 1450 ℃ for 3 h as functions of air pre-sintering temperature.

8YSZ ceramics pre-sintered at different temperatures for 4 h in air and subsequently HIP post-treated at 1450 ℃ for 3 h under 176 MPa Ar. To expose the grain boundaries, the HIP post-treated ceramics were thermally etched at 1200 ℃ for 3 h in a muffle furnace. The relative densities and average grain sizes of HIP post-treated 8YSZ ceramic samples as functions of the pre-sintering temperature are shown in Fig. 8. As shown in Figs. 7(a) and 7(b), a mass of interconnected pores still exist in the 8YSZ ceramic samples pre-sintered at 1250 and 1275 ℃, which is attributed to the penetration of argon through open pores during HIP post-treatment. These remaining pores act as the optical scattering centers, resulting in the opaque and low optical transmittance of 8YSZ ceramics, as shown in Figs. 5 and 6, respectively. The slight grain growth during HIP treatment is ascribed to the pinning effect from those interconnected pores. When the pre-sintering temperature increases to 1280 and 1290 ℃, the HIP post-treated 8YSZ ceramics show almost fully dense structures (relative density > 99.9%), and no visible pores can be observed in Figs. 7(c) and 7(d). The intergranular isolated pores found in the pre-sintered ceramic samples (Figs. 3(c) and 3(d)) were eliminated during HIP post-treatment. In the HIP post-treated 8YSZ ceramic samples pre-sintered at 1300 and 1325 ℃, intragranular pores appear and result in the lower optical transmittance (Fig. 6). As discussed in Eq. (2), the densification rate of ceramics and driving force for closure of isolated pores during HIP post-treatment can be influenced by the grain size of pre-sintered ceramics: The smaller the grain size, the higher driving force for closure of isolated pores is. As can be seen from Figs. 3(e) and 3(f), the 8YSZ ceramic samples pre-sintered at 1300 and 1325 ℃ have larger grain size, which results that some micro-pores are remained in the HIP post-treated ceramics pre-sintered at higher temperatures. For the HIP post-treated 8YSZ ceramics pre-sintered at 1250, 1275, 1280, 1290, 1300, and 1325 ℃, the average grain sizes are 1.6, 1.6, 5.5, 5.6, 5.8, and 5.7 μm, respectively.

Figure 9 demonstrates the thermally-etched surfaces of the 8YSZ ceramics pre-sintered at 1280 ℃ followed by HIP post-treatment at 1350, 1450, and 1550 ℃ for 3 h under 176 MPa Ar. The higher HIP temperature can provide larger driving force to remove pores and promote grain growth. For the 8YSZ ceramics HIP post-treated at 1350 ℃, a few residual pores locate at triple junctions (Fig. 9(a)), which is consistent with their lower optical transmittance shown in Fig. 6(a). The 8YSZ ceramic samples HIP post-treated at 1450 and 1550 ℃ show almost fully dense structures, and no visible pores can be found. With the HIP temperatures increasing from 1350 1450, to 1550 ℃, the average grain size of 8YSZ ceramics increases from 2.4, 5.5 to 16.3 μm.

Figure 10(a) shows the photographs of the 8YSZ transparent ceramics with an increased dimension (36.0 mm in length and 4.0 mm in thickness) pre-sintered at 1280, 1290, and 1300 ℃ and HIP post-

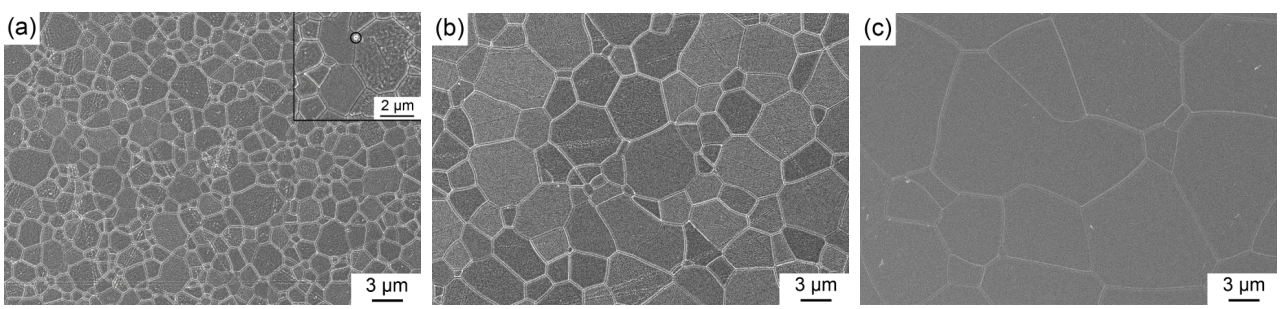

Fig. 9 FESEM micrographs of the thermally-etched surfaces of 8YSZ ceramics pre-sintered at 1280 ℃ for 4 h in air and HIP post-treated at (a) 1350 ℃, (b) 1450 ℃, and (c) 1550 ℃ for 3 h under 176 MPa Ar.

Fig. 10 (a) Photographs of the 8YSZ transparent ceramics (4.0 mm in thickness) pre-sintered at 1280, 1290, and 1300 ℃ for 4 h and HIP post-treated at 1550 ℃ for 3 h, (b) picture of the 8YSZ transparent ceramics (4.0 mm in thickness) pre-sintered at 1280 ℃ (the sample is 100 mm positioned above the background), and (c) in-line transmission curve of the 8YSZ transparent ceramics shown in (b).

treated at 1550 ℃ for 3 h. These large-scaled 8YSZ ceramics still have high optical transparency compared with the smaller ceramics shown in Fig. 5. Meanwhile, Fig. 10(b) shows the picture of the 8YSZ transparent ceramics (4.0 mm in thickness) pre-sintered at 1280 ℃. The letters behind the 8YSZ ceramics can be clearly seen even the sample is 100 mm positioned above the background. Figure 10(c) illustrates the in-line transmission curve of the 8YSZ transparent ceramics shown in Fig. 10(b), and its in-line transmittance at 600 nm reaches 65.9%.

Table 1 summarizes the HIP temperatures, in-line transmittances, average grain sizes, bending strengths, H, and K_{IC} of the 8YSZ transparent ceramics pre-sintered at 1280 ℃ for 4 h and HIP post-treated at 1350, 1450, and 1550 ℃ for 3 h under 176 MPa Ar. The 8YSZ transparent ceramics with the thickness of 2.5 mm were characterized to give the in-line transmittance, and the 8YSZ transparent ceramic bars with the dimensions of 3 mm × 4 mm × 36 mm were characterized to give the mechanical properties. The indentation on the surface of 8YSZ transparent ceramics pre-sintered at 1280 ℃ and HIP post-treated at 1350 ℃ is shown in Fig. 11. It is commonly acknowledged that the residual stress exists in HIP post-treated ceramics [38]. Residual stress can cause a decline in the mechanical properties of ceramics, especially when the dimension of ceramics is larger [39]. All the 8YSZ ceramic bars with the dimensions of 3 mm × 4 mm × 36 mm were annealed at 900 ℃ for 10 h in air prior to testing mechanical properties in order to alleviate the residual stress. With the increase of HIP temperature from 1350 to 1550 ℃, the bending strength of 8YSZ transparent ceramics decreases from 328±20 to 289±19 MPa, H decreases from 12.9±0.1 to 12.5±0.2 GPa, and K_{IC} decreases from 1.30±0.02 to 1.26±0.03 MPa·m$^{1/2}$. It is generally accepted that H decreases with the increase of grain size because of the phenomenon that the grain boundaries can block the dislocations generated by the indenter [30,33,40]. For the 8YSZ transparent ceramics (1 mm in thickness) HIP post-treated at the high-temperature range of 1650–1800 ℃ [17,23–26,41], the in-line transmittance at 600 nm was in the range of 72%–75%, the grain size was larger than 50 μm, and no mechanical properties were reported. For the 8YSZ transparent ceramics (1 mm in thickness) sintered by SPS at the low-temperature range of 1100–1400 ℃ [1,5,6,10,11], the in-line transmittance at 600 nm was in the range of 40%–50%, the average grain size was in the range of 0.2–0.5 μm, and only simple H or K_{IC} was reported. For the 8YSZ transparent ceramics (1.0 mm in thickness) reported in Ref. [34], with the increase of HIP temperature from 1300 to 1500 ℃, the in-line transmittance at 600 nm increased from 57% to 70%, the average grain size increased from 0.7 to 5.0 μm, and the bending strength decreased from 432 to 376 MPa. The in-line transmittance

Table 1 HIP temperatures, in-line transmittances (2.5 mm in thickness), average grain sizes, bending strengths, H, and K_{IC} of the 8YSZ transparent ceramics pre-sintered at 1280 ℃ for 4 h and HIP post-treated at 1350, 1450, and 1550 ℃ for 3 h

HIP temperature (℃)	In-line transmittance at 600 nm (%)	Average grain size (μm)	Bending strength (MPa)	H (GPa)	K_{IC} (MPa·m$^{1/2}$)
1350	56.9	2.4	328±20	12.9±0.1	1.30±0.02
1450	64.7	5.5	314±18	12.7±0.1	1.29±0.02
1550	71.5	16.3	289±19	12.5±0.2	1.26±0.03

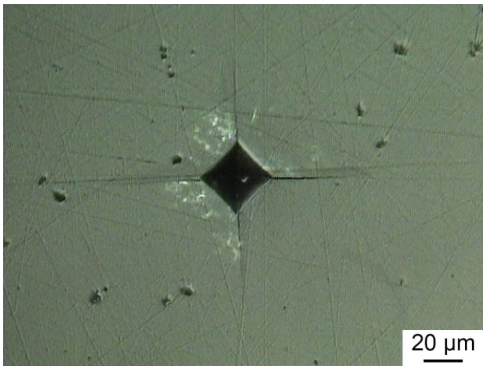

Fig. 11 Indentation on the surface of 8YSZ transparent ceramics pre-sintered at 1280 ℃ for 4 h and HIP post-treated at 1350 ℃ for 3 h.

of the large-sized 8YSZ transparent ceramics prepared in this work is better than that have been reported in Ref. [34].

4 Conclusions

Using the commercial 8YSZ powders as raw material without any sintering additive, 8YSZ transparent ceramics were fabricated by air pre-sintering (1250–1325 ℃) and HIP post-treatment (1350–1550 ℃), which showed high optical and mechanical properties. It is found that the pre-sintering and HIP post-treatment temperatures have great influence on the microstructure, optical transparency, and mechanical properties of 8YSZ ceramics. The 8YSZ ceramic samples pre-sintered at 1280 ℃ have the average grain size of 0.61 μm and the relative density of 93.9%, which provides the optimum microstructure for HIP post-treatment. With the increase of HIP temperature from 1350 to 1550 ℃, the in-line transmittance of 8YSZ ceramics at 600 nm increases from 56.9% to 71.5% (2.5 mm in thickness), and the average grain size increases from 2.4 to 16.3 μm. The corresponding bending strength of 8YSZ transparent ceramics decreases from 328±20 to 289±19 MPa, H decreases from 12.9±0.1 to 12.5±0.2 GPa, and K_{IC} decreases from 1.30±0.02 to 1.26±0.03 MPa·m$^{1/2}$. Finally, 8YSZ transparent ceramics with a larger dimension (36.0 mm in length and 4.0 mm in thickness) were successfully fabricated as well.

Acknowledgements

This work was supported by the National Key R&D Program of China (Grant No. 2021YFE0104800) and the Key Research Project of Frontier Science of Chinese Academy of Sciences (Grant No. QYZDB-SSW- JSC022).

References

[1] Alaniz JE, Perez-Gutierrez FG, Aguilar G, *et al*. Optical properties of transparent nanocrystalline yttria stabilized zirconia. *Opt Mater* 2009, **32**: 62–68.

[2] Li J, Chen PH, Ikesue A. Passive application/window, dome, and armor. In: *Processing of Ceramics: Breakthrough in Optical Ceramics*. Ikesue A, Ed. Hoboken (USA): John Wiley & Sons, 2021: 275–348.

[3] Xiao ZH, Yu SJ, Li YM, *et al*. Materials development and potential applications of transparent ceramics: A review. *Mater Sci Eng R Rep* 2020, **139**: 100518.

[4] Davoodzadeh N, Cano-Velázquez MS, Halaney DL, *et al*. Characterization of ageing resistant transparent nanocrystalline yttria-stabilized zirconia implants. *J Biomed Mater Res B Appl Biomater* 2020, **108**: 709–716.

[5] Paygin V, Stepanov S, Dvilis E, *et al*. Effect of technological parameters on optical and mechanical properties of spark plasma sintered transparent YSZ ceramics. *Ceram Int* 2021, **47**: 11169–11175.

[6] Dash A, Kim BN, Klimke J, *et al*. Transparent tetragonal-cubic zirconia composite ceramics densified by spark plasma sintering and hot isostatic pressing. *J Eur Ceram Soc* 2019, **39**: 1428–1435.

[7] Hříbalová S, Pabst W. Modeling light scattering by spherical pores for calculating the transmittance of transparent ceramics—All you need to know. *J Eur Ceram Soc* 2021, **41**: 2169–2192.

[8] Anselmi-Tamburini U, Woolman JN, Munir ZA. Transparent nanometric cubic and tetragonal zirconia obtained by high-pressure pulsed electric current sintering. *Adv Funct Mater* 2007, **17**: 3267–3273.

[9] Casolco SR, Xu J, Garay JE. Transparent/translucent polycrystalline nanostructured yttria stabilized zirconia with varying colors. *Scripta Mater* 2008, **58**: 516–519.

[10] Zhang HB, Kim BN, Morita K, *et al*. Optimization of high-pressure sintering of transparent zirconia with nano-sized grains. *J Alloys Compd* 2010, **508**: 196–199.

[11] Zhang HB, Kim BN, Morita K, *et al*. Optical properties and microstructure of nanocrystalline cubic zirconia prepared by high-pressure spark plasma sintering. *J Am Ceram Soc* 2011, **94**: 2981–2986.

[12] Peuchert U, Okano Y, Menke Y, *et al*. Transparent cubic-ZrO_2 ceramics for application as optical lenses. *J Eur Ceram Soc* 2009, **29**: 283–291.

[13] Damestani Y, Reynolds CL, Szu J, *et al*. Transparent nanocrystalline yttria-stabilized-zirconia calvarium prosthesis. *Nanomed Nanotechnol Biol Med* 2013, **9**: 1135–1138.

[14] Krell A, Hutzler T, Klimke J. Transmission physics and consequences for materials selection, manufacturing, and applications. *J Eur Ceram Soc* 2009, **29**: 207–221.

[15] Huang XY, Liu YM, Liu Y, *et al*. Fabrication and

characterizations of Yb:YAG transparent ceramics using alcohol–water co-precipitation method. *J Inorg Mater* 2021, **36**: 217–224.

[16] Zhang L, Ben Y, Chen H, *et al*. Low temperature-sintering and microstructure of highly transparent yttria ceramics. *J Alloys Compd* 2017, **695**: 2580–2586.

[17] Tsukuma K, Yamashita I, Kusunose T. Transparent 8 mol% Y_2O_3–ZrO_2 (8Y) ceramics. *J Am Ceram Soc* 2008, **91**: 813–818.

[18] Lee SH, Kupp ER, Stevenson AJ, *et al*. Hot isostatic pressing of transparent Nd:YAG ceramics. *J Am Ceram Soc* 2009, **92**: 1456–1463.

[19] Chen XP, Liu X, Feng YG, *et al*. Microstructure evolution in two-step-sintering process toward transparent Ce:$(Y,Gd)_3(Ga,Al)_5O_{12}$ scintillation ceramics. *J Alloys Compd* 2020, **846**: 156377.

[20] Jin LL, Zhou GH, Shimai S, *et al*. ZrO_2-doped Y_2O_3 transparent ceramics via slip casting and vacuum sintering. *J Eur Ceram Soc* 2010, **30**: 2139–2143.

[21] Liu ZY, Toci G, Pirri A, *et al*. Fabrication, microstructures, and optical properties of Yb:Lu_2O_3 laser ceramics from co-precipitated nano-powders. *J Adv Ceram* 2020, **9**: 674–682.

[22] Li XY, Snetkov IL, Yakovlev A, *et al*. Fabrication and performance evaluation of novel transparent ceramics RE:$Tb_3Ga_5O_{12}$ (RE = Pr, Tm, Dy) toward magneto-optical application. *J Adv Ceram* 2021, **10**: 271–278.

[23] Tsukuma K. Transparent titania–yttria–zirconia ceramics. *J Mater Sci Lett* 1986, **5**: 1143–1144.

[24] Liu Q, Chen PH, Jiang N, *et al*. Fabrication and characterizations of 8.7 mol% Y_2O_3–ZrO_2 transparent ceramics using co-precipitated nanopowders. *Scripta Mater* 2019, **171**: 98–101.

[25] Chen PH, Liu Q, Li XY, *et al*. Influence of terminal pH value on co-precipitated nanopowders for yttria-stabilized ZrO_2 transparent ceramics. *Opt Mater* 2019, **98**: 109475.

[26] Chen PH, Liu Q, Feng YG, *et al*. Transparent $Y_{0.16}Zr_{0.84}O_{1.92}$ ceramics sintered from co-precipitated nanopowder. *Opt Mater* 2020, **100**: 109645.

[27] Permin DA, Boldin MS, Belyaev AV, *et al*. IR-transparent MgO–Gd_2O_3 composite ceramics produced by self-propagating high-temperature synthesis and spark plasma sintering. *J Adv Ceram* 2021, **10**: 237–246.

[28] Tran TB, Hayun S, Navrotsky A, *et al*. Transparent nanocrystalline pure and Ca-doped MgO by spark plasma sintering of anhydrous nanoparticles. *J Am Ceram Soc* 2012, **95**: 1185–1188.

[29] Grasso S, Yoshida H, Porwal H, *et al*. Highly transparent α-alumina obtained by low cost high pressure SPS. *Ceram Int* 2013, **39**: 3243–3248.

[30] Ghanizadeh S, Grasso S, Ramanujam P, *et al*. Improved transparency and hardness in α-alumina ceramics fabricated by high-pressure SPS of nanopowders. *Ceram Int* 2017, **43**: 275–281.

[31] Jiang N, Xie RJ, Liu Q, *et al*. Fabrication of sub-micrometer MgO transparent ceramics by spark plasma sintering. *J Eur Ceram Soc* 2017, **37**: 4947–4953.

[32] Yavetskiy RP, Balabanov AE, Parkhomenko SV, *et al*. Effect of starting materials and sintering temperature on microstructure and optical properties of Y_2O_3:Yb^{3+} 5 at% transparent ceramics. *J Adv Ceram* 2021, **10**: 49–61.

[33] Zhu LL, Park YJ, Gan L, *et al*. Fabrication of transparent Y_2O_3 ceramics with record-high thermal shock resistance. *J Eur Ceram Soc* 2018, **38**: 4050–4056.

[34] Masahiro W, Satoshi K, Koji T. Transparent zirconia sintered body and method for producing same. Europe patent 2 463 257 A1, Jun. 2018.

[35] Zhang Y, Cai M, Jiang BX, *et al*. Micro-structure of grain boundary in post-annealed sinter plus HIPed Nd:$Lu_3Al_5O_{12}$ ceramics. *Opt Mater Express* 2014, **4**: 2182–2189.

[36] Wang ZJ, Wang XJ, Zhou GH, *et al*. Highly transparent yttrium titanate ($Y_2Ti_2O_7$) ceramics from co-precipitated powders. *J Eur Ceram Soc* 2019, **39**: 3229–3234.

[37] Hu DJ, Li XY, Snetkov I, *et al*. Fabrication, microstructure and optical characterizations of holmium oxide (Ho_2O_3) transparent ceramics. *J Eur Ceram Soc* 2021, **41**: 759–767.

[38] Nakao W, Mori S, Nakamura J, *et al*. Self-crack-healing behavior of mullite/SiC particle/SiC whisker multi-composites and potential use for ceramic springs. *J Am Ceram Soc* 2006, **89**: 1352–1357.

[39] Li JM, Zhang BH, Tian R, *et al*. Hot isostatic pressing of transparent AlON ceramics assisted by dissolution of gas inclusions. *J Eur Ceram Soc* 2021, **41**: 4327–4336.

[40] Gan L, Park YJ, Kim H, *et al*. Mechanical properties of submicrometer-grained transparent yttria ceramics by hot pressing with hot-isostatic pressing. *Int J Appl Ceram Technol* 2016, **13**: 678–684.

[41] Yamashita I, Kudo M, Tsukuma K. Development of highly transparent zirconia ceramics. *TOSOH Research & Technology Review* 2012, **56**: 11–16.